ACS APPLIED MATERIALS & INTERFACES
Research Article
www.acsami.org

Sponge-Templated Macroporous Graphene Network for Piezoelectric ZnO Nanogenerator

Xinda Li,[†] Yi Chen,[†] Amit Kumar,[†] Ahmed Mahmoud,[‡] John A. Nychka,[†] and Hyun-Joong Chung*,[†]

[†]Department of Chemical and Materials Engineering, and [‡]Department of Chemistry, University of Alberta, Edmonton, Alberta T6G 2V4, Canada

Supporting Information

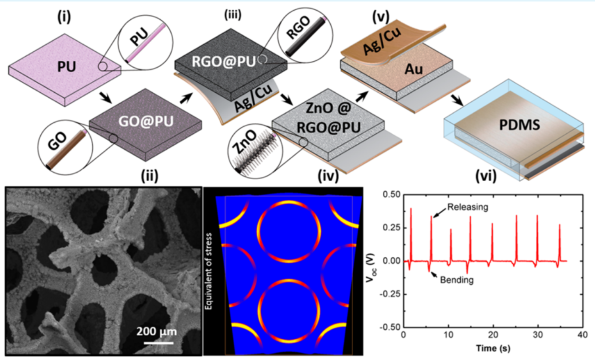

ABSTRACT: We report a simple approach to fabricate zinc oxide (ZnO) nanowire based electricity generators on three-dimensional (3D) graphene networks by utilizing a commercial polyurethane (PU) sponge as a structural template. Here, a 3D network of graphene oxide is deposited from solution on the template and then is chemically reduced. Following steps of ZnO nanowire growth, polydimethylsiloxane (PDMS) backfilling and electrode lamination completes the fabrication processes. When compared to conventional generators with 2D planar geometry, the sponge template provides a 3D structure that has a potential to increase power density per unit area. The modified one-pot ZnO synthesis method allows the whole process to be inexpensive and environmentally benign. The nanogenerator yields an open circuit voltage of ~0.5 V and short circuit current density of ~2 $\mu A/cm^2$, while the output was found to be consistent after ~3000 cycles. Finite element analysis of stress distribution showed that external stress is concentrated to deform ZnO nanowires by orders of magnitude compared to surrounding PU and PDMS, in agreement with our experiment. It is shown that the backfilled PDMS plays a crucial role for the stress concentration, which leads to an efficient electricity generation.

KEYWORDS: *piezoelectric nanogenerator, sponge-templated macroporous network, zinc oxide nanowire, hydrothermal synthesis, reduced graphene oxide*

1. INTRODUCTION

Emerging technology of "Internet of Things (IoT)", a proposed network evolution that all living and nonliving objects have network connectivity to send and receive data, demands power sources to be included in all existing objects.[1] Batteries and solar cells are among possible solutions; however, presumably, consumers do not wish to see an increase in price for inexpensive commodity items. Printed radio frequency identification (RFID) may provide wireless power transmission at the cost of cents per product.[2] When wireless transmission is unavailable to match the power consumption, an additional power device is required, preferably at the lowest production cost possible. Energy harvesting by utilizing piezoelectric materials that can convert mechanical motion to electrical energy is suitable for wearable products, where devices can be charged during daily activities.[3,4]

Originated from seminal contributions by Wang and coworkers,[5−7] arrays of zinc oxide (ZnO) nanowires have been utilized as promising electricity generators by the piezoelectric effect. The piezoelectricity stems from the crystalline structures of the nanowires and their self-rectifying nature at the electrical contact to substrate materials.[8−10] Recent studies suggest that ZnO arrays on graphene provide an attractive option for nanogenerators due to desirable Schottky barrier properties.[11−14] For IoT applications, remaining challenges include a simple and inexpensive synthesis of the nanomaterials and the maximization of the ZnO/graphene area for high-density power generation. The former can be achieved by hydrothermal synthesis of ZnO nanowires, which allows a high density array of ZnO at the maximum processing temperature of ~90 °C.[15,16] The latter requires a three-dimensional (3D) porous network of graphene with a low-cost fabrication method.[17−19]

Recently, an increasing number of studies have demonstrated the adoption of commodity products as structured substrates for growing functional nanomaterials. Use of commodity items allows an inexpensive pathway to produce well-defined hierarchical structures. Established mechanical properties of the substrate material is also an advantage. For example, commercially available foams, sponges, and textiles have been transformed to electrochemical capacitors,[20,21] pressure sensors,[22] antivibration materials,[23] heat insulators,[24] oil absorbents,[25−27] superhydrophobic surfaces,[28] and separating membranes.[29]

Received: June 26, 2015
Accepted: August 19, 2015
Published: August 19, 2015

DOI: 10.1021/acsami.5b05702
ACS Appl. Mater. Interfaces 2015, 7, 20753−20760

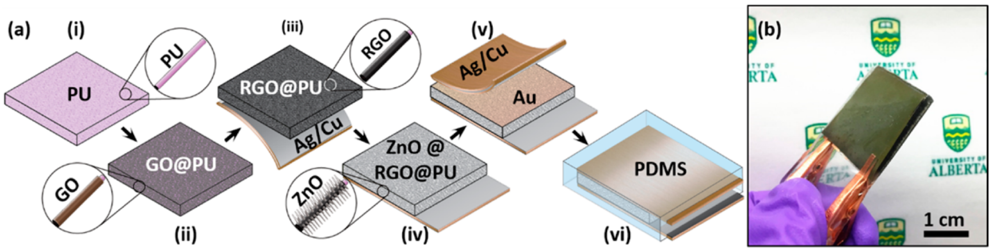

Figure 1. (a) Process of nanogenerator fabrication. (i) Pristine PU sponge. (ii) GO coated on the internal and external surfaces of the PU sponge. (iii) GO reduced by L-AA (RGO); bottom electrode attached. (iv) ZnO nanowires grown on the RGO. (v) Thin layer of sputtered Au on the top of the sample; top electrode attached. (vi) PDMS infused into the pores of the nanogenerator. The insets in the figure illustrate the microstructure of each step. (b) Photo of a fully assembled nanogenerator.

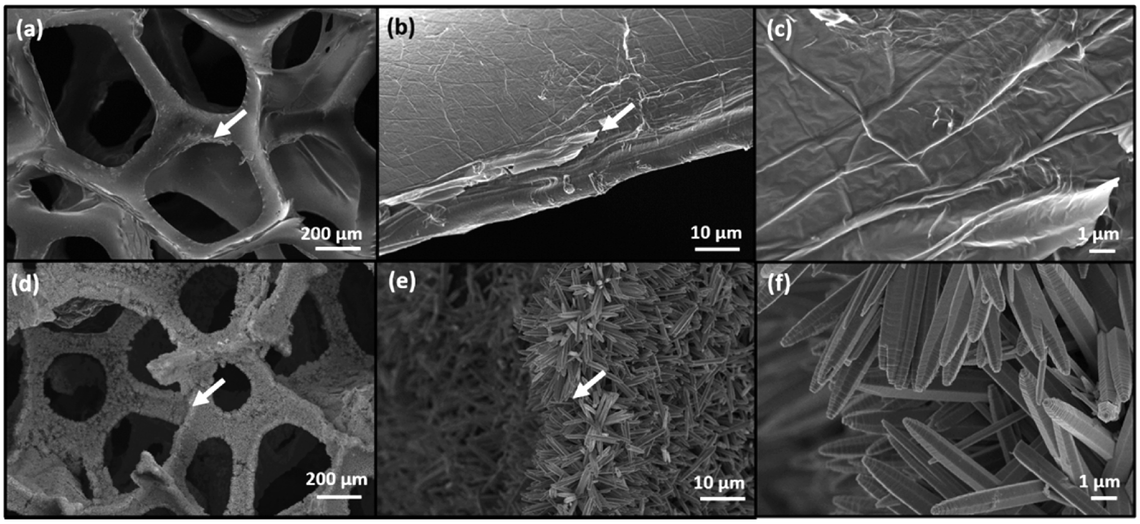

Figure 2. (a−c) SEM images of RGO@PU with different magnification. (d−f) SEM images of ZnO@RGO@PU with different magnification. White arrows indicate the locations for the zoom-in.

Here we present a simple and inexpensive processing pathway to produce a 3D-structured nanogenerator with mechanical integrity. A commercially available polyurethane (PU) sponge was used as a substrate to provide a 3D macroporous network structure and ideal mechanical properties (structural integrity, modulus, and resilience) for the nanogenerator. A graphene coating on the PU sponge was formed by reducing aqueous graphene oxide into a conductive 3D network. We developed a one-step hydrothermal method that grows ZnO nanowires on the graphene network. The whole process was performed in aqueous solution under 95 °C with chemicals that are environmentally benign. The pores were then backfilled with another elastomeric soft material, poly(dimethylsiloxane) (PDMS). The backfilling provided a protection for the nanowires from shedding off during operation. More importantly, the backfilling caused stress localization to the ZnO arrays under operational conditions, as supported by finite element analysis of stress distribution, thus it allowed an effective electricity generation.

2. EXPERIMENTAL SECTION

2.1. Nanogenerator Fabrication. *Graphene Oxide Dip-Coating.* An as-received commercial polyurethane sponge (87035K41, McMaster-Carr, US) with dimension $3 \times 3 \times \sim 0.2$ cm^3 was immersed into graphene oxide (GO) solution (4 mg GO/ml, Graphenea, Spain). Typically, each sample could take up 1.5 mL of GO solution. Then the sponge was dried in a convection oven for 6 h at 80 °C. The mass of sponge after drying process was increased from 59.0 ± 3.4 to 64.3 ± 4.7 mg. The increased mass can be attributed to coated GO.

Graphene Oxide Reduction. We adopted an established protocol of vitamin-C based reduction method.[30,31] The GO coated sponges were reduced using L-ascorbic acid aqueous solution (L-AA, 8 mg/mL, Sigma-Aldrich) solution in oil bath with distillation apparatus at 95 °C. After reaction for 4 h, the sponges were dialyzed in deionized water to remove remaining L-AA. Then the sponges were dried in a convection oven for 6 h at 80 °C. After that, the sponges were attached to copper/Kaptone sheet (DuPont) using silver paste and cured in a convection oven for 6 h at 80 °C. The reduced GO on PU is denoted as RGO@PU.

ZnO Nanorod Synthesis. A ZnO precursor solution was first prepared by dissolving zinc nitrate hexahydrate (80 mM Sigma-Aldrich), hexamethyleneteteramine (HMTA; 25 mM; Sigma-Aldrich), polyethylenimine (PEI; 5 mM; Sigma-Aldrich), and ammonia solution (30%, ACS reagent grade; 5 mL; Sigma-Aldrich) in 100 mL of deionized (DI) water. The solution was stirred at room temperature for 1 h until it became a clear solution.[32] The one-pot synthesis of ZnO nanowire was conducted in 95 °C solution. The RGO@PU was placed on the liquid surface, and the container was closed for 10 min to allow the solution to permeate the entire sponge sample. Then, the cover was open to facilitate precipitation of ZnO seeds due to a sudden vapor pressure drop. A slow agitation of RGO@PU allowed a uniform coating of the ZnO seed on the surface of the porous material. Subsequently, the sample was submerged in the solution and the cover was closed again for ZnO nanowire growth.[33] The as-grown sample was rinsed with DI water and ethanol and then dried for further use. The mass of the sponge after the drying process increased from 64.3 ± 4.7 to 117.2 ± 16.1 mg. The increased mass can be attributed to ZnO nanowires.

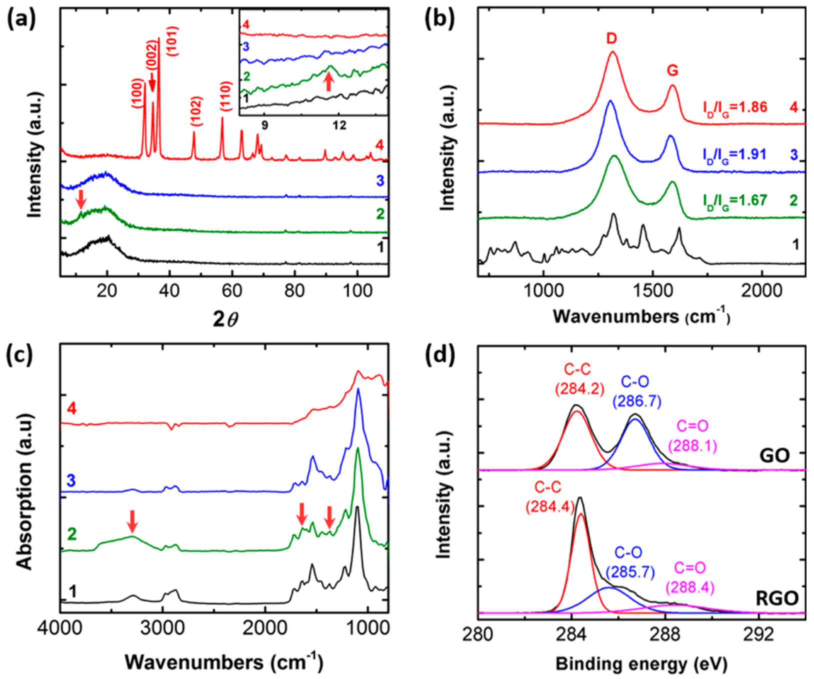

Figure 3. (a) XRD patterns (inset: close look at the low 2θ signals). (b) Raman spectra. (c) FTIR spectra of pristine PU (1), GO@PU (2), RGO@PU (3), and ZnO@RGO@PU (4). (d) XPS spectra of GO and RGO.

Nanogenerator Integration. A 20 nm thick Au layer was coated on ZnO@RGO@PU by gold sputter unit (Denton) for 180 s, followed by attaching another copper/Kaptone sheet. Two copper alligators were clamped to both electrodes to connect the circuit. Finally, a commercial polydimethylsiloxane (PDMS) material, Sylgard 184 (Corning) was infused into the sponge in a vacuum chamber at 9 Torr and 60 °C for 4 h. The final nanogenerator is shown Figure 1a. Physical appearances after each process step are shown in Supporting Information Figure S1.

2.2. Nanogenerator Characterizations. The surface morphology of samples were investigated by field emission scanning electron microscopy (FE-SEM, Zeiss Sigma). X-ray diffraction (XRD) patterns were recorded on a Rigaku RU-200B X-ray diffractometer with a rotating anode X-ray generator using Cu Kα radiation (40 kV, 110 mA). The chemical bonding characteristics among samples were compared via Fourier transform infrared (FTIR, Thermo Nicolet 8700); main bench with an attached Continuum FTIR microscope was used in attenuated total reflection (ATR) mode with a Germanium Slide-On ATR microscope objective. X-ray photoelectron spectroscopy (XPS) was carried out on a Kratos Axis spectrometer with monochromatized Al Kα. C 1s peak at 284.6 eV was used to calibrate all XPS spectra. A Renishaw In Via microscope system was used to collect Raman spectra from samples. A 785 nm high performance diode laser (air cooled) was used as an excitation source. All Raman spectra were measured with a 20× objective with 60 s integration time. The laser power at the sample was 16 ± 0.5 mW. Ultraviolet photoelectron spectroscopy (UPS) spectra were obtained using a helium discharge source at 21.2 eV (He I) on the Kratos Axis Ultra apparatus with a total instrumental broadening of 0.1 eV. Spectra were referenced to the Fermi level of a sputter-cleaned Au sample in contact with the sample, and set as 0 eV. The UV−vis absorption spectra of the ZnO nanowire suspension (0.1 g ZnO in 10 mL DI water) were obtained on a PerkinElmer NIR-UV spectrophotometer.

2.3. Piezoelectricity Measurements. Piezoelectricity (open circuit voltage and short circuit current density) was recorded under periodic flexural stress (0.2 Hz) using a digital source meter (Keithley-2400; background noise controlled at ±0.5 nA) under ambient conditions. The radius of curvature was about 1 cm during bending. Sample durability was tested by a bicycle revolving at 30 rpm. Here, 20 spokes in the rear wheel bend the nanogenerator with a frequency of 10 Hz at a constant force; the output voltages were recorded.

3. RESULTS AND DISCUSSIONS

3.1. Surface Characterizations. The cross sections of RGO@PU and ZnO@RGO@PU are given in Figure 2. The PU sponge has an open cell structure with ∼500 μm pore size. The diameter of PU fiber is ∼150 μm. In Figure 2b, RGO@PU has a rougher surface compared by pristine PU (Figure S2 in the Supporting Information) which indicates the presence of RGO. Upon immersion of RGO coated sponge into L-AA solution at 95 °C, the color of sponge was changed from brown to black immediately. A decrease in the polar functionality on GO has been previously shown to increase the hydrophobicity of RGO.[34] In the water based solution, the altered wettability results in a high affinity of RGO to the hydrophobic PU template. The magnified images (Figure 2c) show a wrinkled surface morphology of the RGO coating on PU. Figure 2d and e shows dense ZnO nanowires which were grown on the surface of RGO. The areal density of ZnO nanowires on RGO@PU surface is estimated to be $(7.1 \pm 0.8) \times 10^7/\mathrm{cm}^2$ with 10.2 ± 1.4 μm length and 855 ± 192 nm in diameter, according to image analysis results (details in Supporting Information Figure S3).

XRD patterns of PU, GO@PU, RGO@PU, and ZnO@RGO@PU are displayed in Figure 3a. GO@PU (2) exhibits a reflection with peak at $2\theta = 11.6°$, which was not observed in PU (1) and RGO@PU (3) patterns. This 11.6° peak is consistent with an interlayer spacing of 0.68 nm of GO sheets, implying that GO was reduced. Typical results from graphite, a peak at $2\theta = 25°$ (correlated to an interlayer spacing of 0.34 nm of graphite),[35] was not observed. XRD pattern of ZnO@RGO@PU (4) confirmed that the as-grown ZnO nanowires were crystalline and all the diffraction peaks can be indexed to ZnO with the hexagonal wurtzite structure (JCPDS No. 75-0576). No typical XRD peaks for graphene were observed,

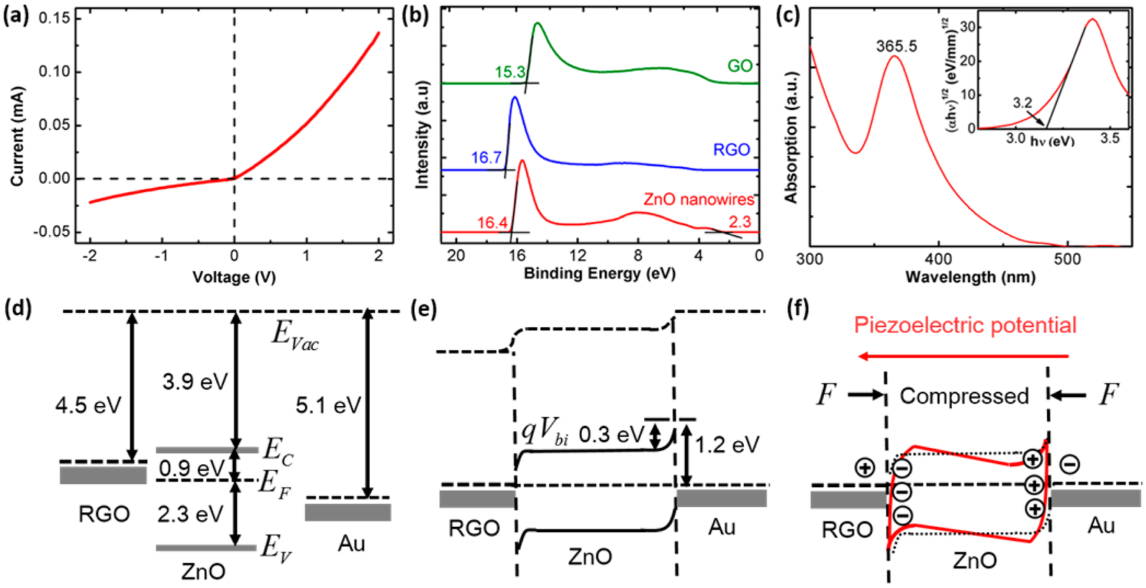

Figure 4. (a) $I-V$ characteristics of nanogenerator. (b) UPS of GO, RGO, and ZnO nanowires. The onset point of UPS spectra were extracted using the linear extrapolation method shown in the figure, which are 15.3, 16.7, and 16.4 eV for GO, RGO, and ZnO nanowires, respectively. Spectra were referenced to the Fermi level of a sputter-cleaned Au sample in contact with the samples, and set as 0 eV. The data indicated that the work functions of GO, RGO and ZnO nanowires are 5.9, 4.5, and 4.8 eV, respectively. The valence band edge energy of ZnO nanowires is 2.3 eV and the valence band maximum can be calculated to be 7.1 eV.[46] (c) UV−vis spectra of ZnO nanowires. The optical band gap is determined by the inset of the Tauc plot, which is 3.2 eV. Band diagrams of Au/ZnO/RGO junction (d) before and (e) after contact formation. The direction of forward bias is defined as from Au to ZnO nanowires. (f) Band diagram of Au/ZnO/RGO junction with stress. The ionic charges in ZnO are due to piezoelectric polarization and the charges in RGO and Au are due to Coulombic interaction.

which is due to the relatively low volumetric content of graphene compared to ZnO nanowires.

Raman spectroscopy was used to determine the structure of GO@PU and RGO@PU. There are two distinguishable bands in Figure 3b. The D-mode (disordered band) is located between 1330 and 1360 cm^{-1}. The G-mode (tangential mode) which corresponds to the stretching mode in the graphite plane is located at 1580 cm^{-1}.[36,37] The relative intensity of D-mode and G-mode depends strongly on the amount of disorder in the graphitic material.[38−40] The intensity ratio of D and G changed from 1.67 in GO to 1.91 in RGO@PU, which indicates a decrease in the average size of the sp^2 domains upon GO reduction.[34] This phenomenon was previously reported in GO reduction using reducing agent.[31,30,34] It is notable that the peaks from PU did not appear in GO or RGO contained samples because of the screening effect of graphitic materials.[41]

FTIR results (Figure 3c) are also in agreement with the conclusion that the GO was successfully reduced. The observation is supported from the following peaks: the broad IR adsorption from 3050 to 3800 cm^{-1} (hydroxyl groups with C−OH vibrations from carboxyl acid), about 1720 cm^{-1} (C=O stretching vibrations from carbonyl and carboxyl groups), 1400 cm^{-1} (O−H bending vibrations from hydroxyl groups), and between 1300 and 1350 cm^{-1} (C−OH stretching vibrations).[31,42] The absorption of the bands associated with oxygen functional groups is strongly decreased in RGO@PU spectrum.

Reduction of GO was further confirmed by XPS. Figure 3d shows the C 1s XPS spectra of GO and RGO. Before reduction, three peaks centered at 284.4, 286.7, and 288.1 eV were detected, whereas each peak corresponds to C=C/C−C (in aromatic rings), C−O, and C=O, respectively.[43] After the reduction, the intensities of C−O and C=O decreased dramatically. The areal ratio of the C 1s peak the O 1s peak with a correction by atomic sensitivity factors (0.25 for C 1s and 0.66 for O 1s), allows an estimation of the atomic ratio in the material. In our experiment, the ratio of carbon to oxygen was 1.7 for GO and 6.2 for RGO (4 h reduction), which can be described as an evidence for highly reduced graphene oxide.[44]

The resistances of GO@PU and RGO@PU were also measured. Samples with dimension 3 × 3 × ∼ 0.2 cm^3 were sandwiched between two copper electrodes. The resistance of GO@PU and RGO@PU was 674 ± 69 kΩ and 26.7 ± 3.9 Ω, respectively. The 4 orders of magnitude improvement in conductivity indicates GO was reduced to RGO.

3.2. Piezoelectricity Measurements. Figure 4a shows the current−voltage ($I-V$) behavior of the nanogenerator at zero strain. The asymmetric $I-V$ curve implies the rectifying behavior, which stems from the differences in electrical contact at the ZnO/RGO and the ZnO/Au interfaces. The UPS spectra in Figure 4b reveals valence energy levels of GO, RGO and ZnO nanowires with respect to the source emission line (He 1α; 21.2 eV). The valence band maximum and work function of ZnO nanowires were 7.1 and 4.8 eV, respectively. The optical band gap of ZnO nanowires was determined by UV−vis spectrum in Figure 4c, which was 3.2 eV. Then, the conduction band minimum of ZnO was calculated using valence band maximum subtracted by band gap, which equals to 3.9 eV. The obtained values of ZnO nanowires are similar to those reported in literature.[45,46] The work function of RGO is 4.5 eV probed by UPS, which is larger than the reported work function of graphene prepared by chemical vapor deposition method.[47] Kumar et al. reported that the oxygen-containing functionalities have a decisive influence on RGO work function.[48] Incorporation of electron withdrawing groups such as hydroxyl, carboxyl and epoxy in graphene increases the work function and the increment is proportional to the final oxygen concentration in RGO. In our case, experimental results show

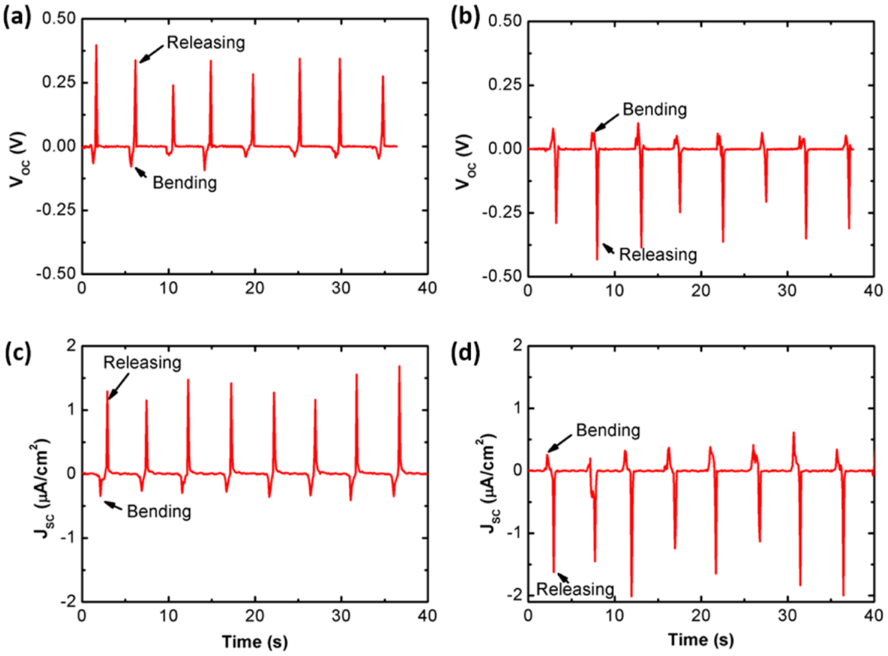

Figure 5. Open circuit voltage measured from nanogenerator by (a) forward and (b) reverse connections. Short circuit current density measured from nanogenerator by (c) forward and (d) reverse connections.

the oxygen concentration of GO dropped from 37% to 14%, and work function decreases from 5.9 to 4.5 eV. An energy band diagram of nanogenerator is illustrated in Figure 4d. The mismatch between the work functions of ZnO and Au causes a band bending, which results in an energy barrier for electrons from Au to ZnO of 1.2 eV (Figure 4e). On the other side of the contact, ZnO nanowires has an ohmic contact with RGO. When the forward bias is applied, the Fermi level of Au is lower than that of ZnO. The energy barrier is decreased for electrons to transport from ZnO nanowires to Au, leading to a forward bias current in the nanogenerator. When the reverse bias is applied, the Fermi level of Au is raised above that of ZnO nanowires. The Schottky barrier blocks the flow of electrons from Au to ZnO causing the observed rectifying behavior.

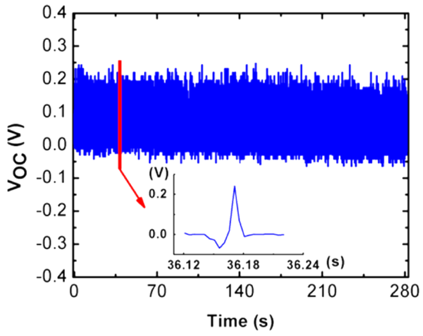

Figure 6. Output voltages recorded when the rear wheel was revolving at 30 rpm.

Figure 5a and c shows the open circuit voltage and short circuit current density measured from the nanogenerator. Upon bending with the frequency of 0.2 Hz (i.e., bending every 5 s; see the video in the Supporting Information), the nanogenerator yielded an open circuit voltage ranging between 0.25 and 0.41 V and a short circuit current density ranging between 1.18 and 1.70 μA/cm². The nanogenerator showed negative and positive peaks when bent and released because of charging and discharging, respectively. The asymmetricity between bending and releasing in voltage and current outputs are because releasing happens quicker than bending in our experiment.[49] A switching polarity test (Figure 5b and d) of the nanogenerator was conducted for forward and reverse connections to confirm that the measured signals originated from the piezoelectric effect, not an artifact from the measurement system. The nanogenerator yielded open circuit voltage ranging between −0.23 and −0.45 V and short circuit current density ranging between −1.20 and −2.05 μA/cm². When the nanogenerator was bent, immobile ionic charges were created in ZnO nanowires (Figure 4f). The piezoelectric potential will attract and accumulate countercharges in the Au and RGO adjacent ZnO.[5,50,51] These charges generate the induced potential in the Au and RGO, resulting in negative peaks in Figure 5a and 5c. When the ZnO nanowires are released, the piezoelectric potential will disappear, and accumulated electrons in Au will flow to RGO through external circuit because electrons are not able to surmount the Schottky barrier at the interface of ZnO and nanowires. It is known that the output behavior of nanogenerator also depends on the bending and releasing rates because the amount of accumulated electrons can be related to the lifetime of piezoelectric potential. However, in our case, dielectric relaxation time (3.5 ms for Au nanoparticle with 50 nm diameter[52]) is three magnitudes smaller than the manual bending rate (5 s/cycle), thus accumulated electrons will screen the piezoelectric potential before the external force is released.

The performance of nanogenerator described in the current paper can be further improved by resolving following challenges. First, the conductivity of RGO is not high, which reduces the efficiency of charge transportation to current collector. It is notable that, in case reduced graphene oxide's conductivity is not high enough, the similar pattern of output voltage and current with that of rectifying device without relation to rectifying effect is possible. In our study, however,

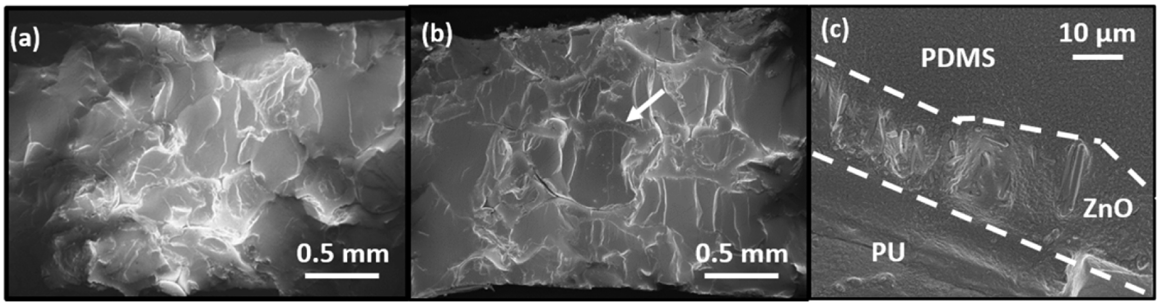

Figure 7. (a) Cross section of the nanogenerator before the durability test. (b) Cross section of the nanogenerator after ∼3000 cycles. White arrows indicate the locations for the zoom-in. (c) Zoomed-in image at PDMS/ZnO nanowires/PU interfaces. White dotted lines show the boundaries of PDMS/ZnO and PU/ZnO.

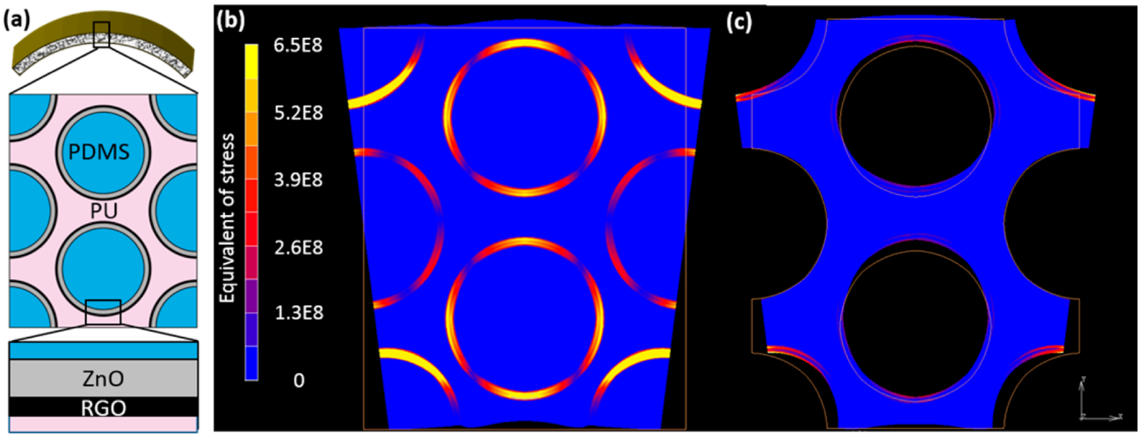

Figure 8. (a) Illustration of the structure of nanogenerator. RGO layer is not included in the FEM model due to its small thickness. (b) FEM simulation for the stress distribution in the nanogenerator with PDMS and (c) without PDMS.

the rectification effect seems to be a real result, as evidenced in Figure 4. Second, the protocol for Au layer coating must be improved to achieve a complete coverage on the other side (i.e., the opposite side from RGO). Third, the synthesis of ZnO nanowires can further be improved to achieve ultrahigh-density nanowires with orientation exactly perpendicular to the local sponge surface. Fourth, poling process may further improve the performance. Fifth, the sponge we used had a large fraction of the porosities; an optimal pore size and porosity needs to be explored in future studies.

3.3. Durability Test. The durability of the nanogenerator was tested using a bicycle. The output voltages were recorded in Figure 6 when the rear wheel was revolving at the speed of 30 rpm. In each peak, the output from nanogenerator exhibited minimum voltage peaks (bending) that range between −0.06 and −0.01 V, whereas the maximum voltage peaks (releasing) range between +0.17 and +0.25 V. The inset in Figure 6 shows a single cycle which was about 0.1 s. Because the radius of curvature bent by spokes is larger than that which is manually bent, the maximum output voltage of bicycle test was smaller compared to Figure 5. After 2800 bending and releasing cycles there were no distinguishable decays in open circuit voltage. Figure 7a and b shows the cross sections of nanogenerator before and after ∼3000 cycle of bicycle-test. The SEM images further confirm that the device was not degraded during operation. Delamination at the interface between hard (ZnO and graphene) and soft (PU and PDMS) materials was not found (Figure 7c), suggesting that PDMS prevents the spallation of ZnO nanorods during repeated reversed bending in the durability test.

3.4. Finite Element Analysis of Macroporous Structure. Since the output voltage is closely related to how the ZnO nanowires are deformed with external force, a finite element method (FEM) simulation program (Marc, MSC Software Corporation) was used to estimate how the stress is distributed in the nanogenerator. We designed a 2D plate model with the dimension of 1.6 mm by 2 mm. The geometry of the nanogenerator cross-section is illustrated in Figure 8a. In our devices, the volume fraction of RGO is relative low, thus we included ZnO nanowires, PU and PDMS into consideration.

Table 1. Material Parameters in FEM Simulation

materials[ab]	Young's modulus	Poisson's ratio	thickness
PU[53]	10 MPa	0.50	
PDMS[54]	3 MPa	0.50	
ZnO[55]	30 GPa	0.35	10 μm[bc]

[a] All materials are considered isotropic to simplify the model. [b] RGO layer is not included for relative low content and small thickness. [c] The layer of ZnO nanowires are considered as a uniform layer. The thicknesses were obtained by SEM imaging.

The material parameters are given in Table 1. To simplify the model, all materials were considered to be isotropic and uniform. The boundary condition during the bending process is described in Supporting Information S4. Briefly, the displacement of the plate boundary was calculated and assigned to boundary elements by the bending curvature with the assumption of pure bending mode. Figure 8b and c shows the simulation results of nanogenerator with and without

PDMS, respectively. With the presence of PDMS backfilling, Figure 8b shows the equivalent stress of ZnO nanowire layer is four magnitudes larger than that in PU and PDMS. However, the stress is not concentrated on ZnO nanowires (Figure 8c). The measured open circuit voltage from nanogenerator without backfilled PDMS is shown in Supporting Information Figure S5. Here, the open circuit voltages (upon release) yielded values ranging from +0.012 to +0.017 V, which are about 20 times smaller than those with backfilled PDMS (cf., Figure 5a). The difference indicates that the role of PDMS is not only a protection for ZnO nanowires, but also an effective stress concentrator for the nanogenerator.

4. CONCLUSIONS

We demonstrated a low temperature processing method to fabricate a ZnO nanowire based electricity generator with a 3D structure templated on a commodity sponge material. GO was dip-coated from aqueous solution on the commodity sponge and reduced by L-AA, resulting in the transformation of a PU sponge into a conductive 3D network. Then, ZnO nanowires were grown by a one-step hydrothermal method in anaqueous solution below 95 °C. The mechanism of piezoelectricity and the band structure of our device were discussed over a band diagram that shows a Schottky contact at the ZnO/Au interface and ohmic contact at the ZnO/RGO interface. The diagram explained the self-rectification and the output mechanism of the piezoelectric nanogenerator. The nanogenerator yielded open circuit voltage range up to ∼0.5 V and short circuit current density range up to ∼2 μA/cm^2, upon bending every 5 s. In an improvised durability test, degradation in output voltage was not found after ∼3000 bending and releasing cycles. Finally, finite element analysis of stress distribution showed that the stress is localized to the ZnO arrays under operational condition within the presence of PDMS, thus allowing effective electricity generation. The novel and environmentally benign processing route that produced high-performance nanogenerator opens up the possibility for industrial scale production.

■ ASSOCIATED CONTENT

Ⓢ Supporting Information

The Supporting Information is available free of charge on the ACS Publications website at DOI: 10.1021/acsami.5b05702.

> Physical appearances of samples after each process step, SEM image of a pristine PU sponge, image analysis results of ZnO nanowires, details of finite element analysis and output performance of nanogenerator without PDMS (PDF)
>
> Video showing bending of nanogenerator at a frequency of 0.2 Hz (AVI)

■ AUTHOR INFORMATION

Corresponding Author

*E-mail: chung.hj13@ualberta.ca. Phone: +1-780-492-4790.

Author Contributions

X.L. and H.-J.C. conceived ideas. X.L., Y.C., and A.K. performed experiments. Y.C., J.A.N., and H.-J.C. established ZnO nanowire array deposition protocols. A.M. provided important contributions in material characterization. X.L. and H.-J.C. wrote manuscript. All authors have given approval to the final version of the manuscript.

Notes

The authors declare no competing financial interest.

■ ACKNOWLEDGMENTS

We thank Prof. Mark McDermott for allowing use of Raman spectroscopy. Other materials imaging and characterizations were performed at the NanoFAB at the University of Alberta. This work was supported by Natural Sciences and Engineering Research Council of Canada (NSERC) and Canadian Institutes of Health Research (CIHR). The use of the logo in Figure 1b is done with the permission of the University of Alberta.

■ REFERENCES

(1) The Internet of Things. *MIT Technology Review Business Report* 2014, July/August.

(2) Zhan, Y.; Mei, Y.; Zheng, L. Materials Capability and Device Performance in Flexible Electronics for the Internet of Things. *J. Mater. Chem. C* **2014**, *2*, 1220−1232.

(3) Talemi, P.; Delaigue, M.; Murphy, P.; Fabretto, M. Flexible Polymer-on-polymer Architecture for Piezo/pyroelectric Energy Harvesting. *ACS Appl. Mater. Interfaces* **2015**, *7*, 8465−8471.

(4) Saravanakumar, B.; Thiyagarajan, K.; Alluri, N. R.; SoYoon, S.; Taehyun, K.; Lin, Z.-H.; Kim, S.-J. Fabrication of an Eco-friendly Composite Nanogenerator for Self-powered Photosensor Applications. *Carbon* **2015**, *84*, 56−65.

(5) Wang, Z. L. Towards Self-Powered Nanosystems: From Nanogenerators to Nanopiezotronics. *Adv. Funct. Mater.* **2008**, *18*, 3553−3567.

(6) Song, J.; Zhou, J.; Wang, Z. L. Piezoelectric and Semiconducting Coupled Power Generating Process of a Single ZnO belt/wire. A Technology for Harvesting Electricity from the Environment. *Nano Lett.* **2006**, *6*, 1656−1662.

(7) Wang, Z. L.; Song, J. Piezoelectric Nanogenerators Based on Zinc Oxide Nanowire Arrays. *Science* **2006**, *312*, 242−246.

(8) Shin, S.-H.; Kim, Y.-H.; Lee, M. H.; Jung, J.-Y.; Seol, J. H.; Nah, J. Lithium-Doped Zinc Oxide Nanowires-Polymer Composite for High Performance Flexible Piezoelectric Nanogenerator. *ACS Nano* **2014**, *8*, 10844−10850.

(9) Hasan, M. R.; Baek, S.-H.; Seong, K. S.; Kim, J. H.; Park, I.-K. Hierarchical ZnO Nanorods on Si Micropillar Arrays for Performance Enhancement of Piezoelectric Nanogenerators. *ACS Appl. Mater. Interfaces* **2015**, *7*, 5768−5774.

(10) Hu, C. J.; Lin, Y. H.; Tang, C. W.; Tsai, M. Y.; Hsu, W. K.; Kuo, H. F. ZnO-Coated Carbon Nanotubes: Flexible Piezoelectric Generators. *Adv. Mater.* **2011**, *23*, 2941−2945.

(11) Kumar, B.; Lee, K. Y.; Park, H.-K.; Chae, S. J.; Lee, Y. H.; Kim, S.-W. Controlled Growth of Semiconducting Nanowire, Nanowall, and Hybrid Nanostructures on Graphene for Piezoelectric Nanogenerators. *ACS Nano* **2011**, *5*, 4197−4204.

(12) Choi, D.; Choi, M. Y.; Choi, W. M.; Shin, H. J.; Park, H. K.; Seo, J. S.; Park, J.; Yoon, S. M.; Chae, S. J.; Lee, Y. H.; et al. Fully Rollable Transparent Nanogenerators Based on Graphene Electrodes. *Adv. Mater.* **2010**, *22*, 2187−2192.

(13) Shin, D.-M.; Tsege, E. L.; Kang, S. H.; Seung, W.; Kim, S.-W.; Kim, H. K.; Hong, S. W.; Hwang, Y.-H. Freestanding ZnO Nanorod/Graphene/ZnO Nanorod Epitaxial Double Heterostructure for Improved Piezoelectric Nanogenerators. *Nano Energy* **2015**, *12*, 268−277.

(14) Nam, G.-H.; Baek, S.-H.; Cho, C.-H.; Park, I.-K. A Flexible and Transparent Graphene/ZnO Nanorod Hybrid Structure Fabricated by Exfoliating a Graphite Substrate. *Nanoscale* **2014**, *6*, 11653−11658.

(15) Chevalier-César, C.; Capochichi-Gnambodoe, M.; Leprince-Wang, Y. Growth Mechanism Studies of ZnO Nanowire Arrays via Hydrothermal Method. *Appl. Phys. A: Mater. Sci. Process.* **2014**, *115*, 953−960.

(16) Chang, H.; Sun, Z.; Ho, K. Y.-F.; Tao, X.; Yan, F.; Kwok, W.-M.; Zheng, Z. A Highly Sensitive Ultraviolet Sensor based on a Facile in situ Solution-Grown ZnO Nanorod/Graphene Heterostructure. *Nanoscale* **2011**, *3*, 258−264.

(17) Lee, S. H.; Kim, H. W.; Hwang, J. O.; Lee, W. J.; Kwon, J.; Bielawski, C. W.; Ruoff, R. S.; Kim, S. O. Three-Dimensional Self-

Assembly of Graphene Oxide Platelets into Mechanically Flexible Macroporous Carbon Films. *Angew. Chem., Int. Ed.* **2010**, *49*, 10084−10088.

(18) Maiti, U. N.; Lim, J.; Lee, K. E.; Lee, W. J.; Kim, S. O. Three-Dimensional Shape Engineered, Interfacial Gelation of Reduced Graphene Oxide for High Rate, Large Capacity Supercapacitors. *Adv. Mater.* **2014**, *26*, 615−619.

(19) Lee, W. J.; Maiti, U. N.; Lee, J. M.; Lim, J.; Han, T. H.; Kim, S. O. Nitrogen-Doped Carbon Nanotubes and Graphene Composite Structures for Energy and Catalytic Applications. *Chem. Commun.* **2014**, *50*, 6818−6830.

(20) Yu, G.; Hu, L.; Vosgueritchian, M.; Wang, H.; Xie, X.; McDonough, J. R.; Cui, X.; Cui, Y.; Bao, Z. Solution-Processed Graphene/MnO2 Nanostructured Textiles for High-Performance Electrochemical Capacitors. *Nano Lett.* **2011**, *11*, 2905−2911.

(21) Yang, Z. Y.; Jin, L. J.; Lu, G. Q.; Xiao, Q. Q.; Zhang, Y. X.; Jing, L.; Zhang, X. X.; Yan, Y. M.; Sun, K. N. Sponge-Templated Preparation of High Surface Area Graphene with Ultrahigh Capacitive Deionization Performance. *Adv. Funct. Mater.* **2014**, *24*, 3917−3925.

(22) Samad, Y. A.; Li, Y.; Schiffer, A.; Alhassan, S. M.; Liao, K. Graphene Foam Developed with a Novel Two-Step Technique for Low and High Strains and Pressure-Sensing Applications. *Small* **2015**, *11*, 2380−2385.

(23) Malakooti, M. H.; Hwang, H.-S.; Sodano, H. A. Morphology-Controlled ZnO Nanowire Arrays for Tailored Hybrid Composites with High Damping. *ACS Appl. Mater. Interfaces* **2015**, *7*, 332−339.

(24) Hsu, P.-C.; Liu, X.; Liu, C.; Xie, X.; Lee, H. R.; Welch, A. J.; Zhao, T.; Cui, Y. Personal Thermal Management by Metallic Nanowire-Coated Textile. *Nano Lett.* **2015**, *15*, 365−371.

(25) Zhang, J.; Seeger, S. Polyester Materials with Superwetting Silicone Nanofilaments for Oil/Water Separation and Selective Oil Absorption. *Adv. Funct. Mater.* **2011**, *21*, 4699−4704.

(26) Liu, Y.; Ma, J.; Wu, T.; Wang, X.; Huang, G.; Liu, Y.; Qiu, H.; Li, Y.; Wang, W.; Gao, J. Cost-Effective Reduced Graphene Oxide-Coated Polyurethane Sponge as a Highly Efficient and Reusable Oil-Absorbent. *ACS Appl. Mater. Interfaces* **2013**, *5*, 10018−10026.

(27) Calcagnile, P.; Fragouli, D.; Bayer, I. S.; Anyfantis, G. C.; Martiradonna, L.; Cozzoli, P. D.; Cingolani, R.; Athanassiou, A. Magnetically Driven Floating Foams for the Removal of Oil Contaminants from Water. *ACS Nano* **2012**, *6*, 5413−5419.

(28) Liu, H. d.; Liu, Z. y.; Yang, M. b.; He, Q. Surperhydrophobic Polyurethane Foam Modified by Graphene Oxide. *J. Appl. Polym. Sci.* **2013**, *130*, 3530−3536.

(29) Zhu, Q.; Chu, Y.; Wang, Z.; Chen, N.; Lin, L.; Liu, F.; Pan, Q. Robust Superhydrophobic Polyurethane Sponge as a Highly Reusable Oil-Absorption Material. *J. Mater. Chem. A* **2013**, *1*, 5386−5393.

(30) Zhang, J.; Yang, H.; Shen, G.; Cheng, P.; Zhang, J.; Guo, S. Reduction of Graphene Oxide via L-Ascorbic Acid. *Chem. Commun.* **2010**, *46*, 1112−1114.

(31) Fernandez-Merino, M.; Guardia, L.; Paredes, J.; Villar-Rodil, S.; Solis-Fernandez, P.; Martinez-Alonso, A.; Tascon, J. Vitamin C is an Ideal Substitute for Hydrazine in the Reduction of Graphene Oxide Suspensions. *J. Phys. Chem. C* **2010**, *114*, 6426−6432.

(32) Liu, K.; Wu, W.; Chen, B.; Chen, X.; Zhang, N. Continuous Growth and Improved PL Property of ZnO Nanoarrays with Assistance of Polyethylenimine. *Nanoscale* **2013**, *5*, 5986−5993.

(33) Baxter, J. B.; Aydil, E. S. Nanowire-based Dye-Sensitized Solar Cells. *Appl. Phys. Lett.* **2005**, *86*, 053114.

(34) Stankovich, S.; Dikin, D. A.; Piner, R. D.; Kohlhaas, K. A.; Kleinhammes, A.; Jia, Y.; Wu, Y.; Nguyen, S. T.; Ruoff, R. S. Synthesis of Graphene-Based Nanosheets via Chemical Reduction of Exfoliated Graphite Oxide. *Carbon* **2007**, *45*, 1558−1565.

(35) Zhang, K.; Zhang, L. L.; Zhao, X. S.; Wu, J. Graphene/Polyaniline Nanofiber Composites as Supercapacitor Electrodes. *Chem. Mater.* **2010**, *22*, 1392−1401.

(36) Casiraghi, C.; Hartschuh, A.; Qian, H.; Piscanec, S.; Georgi, C.; Fasoli, A.; Novoselov, K. S.; Basko, D. M.; Ferrari, A. C. Raman Spectroscopy of Graphene Edges. *Nano Lett.* **2009**, *9*, 1433−1441.

(37) Kudin, K. N.; Ozbas, B.; Schniepp, H. C.; Prud'homme, R. K.; Aksay, I. A.; Car, R. Raman Spectra of Graphite Oxide and Functionalized Graphene Sheets. *Nano Lett.* **2008**, *8*, 36−41.

(38) Ferrari, A. C.; Robertson, J. Interpretation of Raman Spectra of Disordered and Amorphous Carbon. *Phys. Rev. B: Condens. Matter Mater. Phys.* **2000**, *61*, 14095−14107.

(39) Ferrari, A. C.; Robertson, J. Resonant Raman Spectroscopy of Disordered, Amorphous, and Diamondlike Carbon. *Phys. Rev. B: Condens. Matter Mater. Phys.* **2001**, *64*, 13.

(40) Graf, D.; Molitor, F.; Ensslin, K.; Stampfer, C.; Jungen, A.; Hierold, C.; Wirtz, L. Spatially Resolved Raman Spectroscopy of Single- and Few-Layer Graphene. *Nano Lett.* **2007**, *7*, 238−242.

(41) Xia, H.; Song, M. Preparation and Characterization of Polyurethane−Carbon Nanotube Composites. *Soft Matter* **2005**, *1*, 386−394.

(42) Acik, M.; Lee, G.; Mattevi, C.; Chhowalla, M.; Cho, K.; Chabal, Y. Unusual Infrared-Absorption Mechanism in Thermally Reduced Graphene Oxide. *Nat. Mater.* **2010**, *9*, 840−845.

(43) Dreyer, D. R.; Park, S.; Bielawski, C. W.; Ruoff, R. S. The Chemistry of Graphene Oxide. *Chem. Soc. Rev.* **2010**, *39*, 228−240.

(44) Compton, O. C.; Nguyen, S. T. Graphene Oxide, Highly Reduced Graphene Oxide, and Graphene: Versatile Building Blocks for Carbon-Based Materials. *Small* **2010**, *6*, 711−723.

(45) Hwang, J. O.; Lee, D. H.; Kim, J. Y.; Han, T. H.; Kim, B. H.; Park, M.; No, K.; Kim, S. O. Vertical ZnO Nanowires/Graphene Hybrids for Transparent and Flexible Field Emission. *J. Mater. Chem.* **2011**, *21*, 3432−3437.

(46) Feng, W.; Rangan, S.; Cao, Y.; Galoppini, E.; Bartynski, R. A.; Garfunkel, E. Energy Level Alignment of Polythiophene/ZnO Hybrid Solar Cells. *J. Mater. Chem. A* **2014**, *2*, 7034−7044.

(47) Kwon, K. C.; Choi, K. S.; Kim, S. Y. Increased Work Function in Few-Layer Graphene Sheets via Metal Chloride Doping. *Adv. Funct. Mater.* **2012**, *22*, 4724−4731.

(48) Kumar, P. V.; Bernardi, M.; Grossman, J. C. The Impact of Functionalization on the Stability, Work Function, and Photoluminescence of Reduced Graphene Oxide. *ACS Nano* **2013**, *7*, 1638−1645.

(49) Park, K. I.; Lee, M.; Liu, Y.; Moon, S.; Hwang, G. T.; Zhu, G.; Kim, J. E.; Kim, S. O.; Kim, D. K.; Wang, Z. L.; Lee, K. J. Flexible Nanocomposite Generator Made of BaTiO3 Nanoparticles and Graphitic Carbons. *Adv. Mater.* **2012**, *24*, 2999−3004.

(50) Yang, S.; Wang, L.; Tian, X.; Xu, Z.; Wang, W.; Bai, X.; Wang, E. The Piezotronic Effect of Zinc Oxide Nanowires Studied by In Situ TEM. *Adv. Mater.* **2012**, *24*, 4676−4682.

(51) Wang, Z. L. *Piezotronics and Piezo-Phototronics*; Springer: Berlin, Heidelberg, 2013.

(52) Abdelhalim, M. A. K.; Mady, M. M.; Ghannam, M. M. Dielectric Constant, Electrical Conductivity and Relaxation Time Measurements of Different Gold Nanoparticle Sizes. *Int. J. Math., Phys. Eng. Sci.* **2011**, *6*, 5487−5491.

(53) Chizhik, S. A.; Huang, Z.; Gorbunov, V. V.; Myshkin, N. K.; Tsukruk, V. V. Micromechanical Properties of Elastic Polymeric Materials As Probed by Scanning Force Microscopy. *Langmuir* **1998**, *14*, 2606−2609.

(54) Johnston, I.; McCluskey, D.; Tan, C.; Tracey, M. Mechanical Characterization of Bulk Sylgard 184 for Microfluidics and Microengineering. *J. Micromech. Microeng.* **2014**, *24*, 035017.

(55) Ni, H.; Li, X. D. Young's Modulus of ZnO Nanobelts Measured using Atomic Force Microscopy and Nanoindentation Techniques. *Nanotechnology* **2006**, *17*, 3591−3597.